A Yeast-Based High-Throughput Screening Platform for the Discovery of Novel pre-mRNA Splicing Modulators

Sierra L. Love[1,2], Henrik Vollmer[2], Ya-Chu Chang[3,4], Joshua C. Paulson[2], Tucker J. Carrocci[2], Melissa S. Jurica[5], Hai Dang Nguyen[3,4], and Aaron A. Hoskins[2,6]

[1]Genetics Training Program, University of Wisconsin-Madison, Madison, WI 53706
[2]Department of Biochemistry, University of Wisconsin-Madison, Madison, WI 53706
[3]Department of Pharmacology, University of Minnesota, Minneapolis, MN 55455
[4]Masonic Cancer Center, University of Minnesota, Minneapolis, MN 55455
[5]Center for Molecular Biology of RNA, University of California-Santa Cruz, Santa Cruz, CA 95064
[6]Department of Chemistry, University of Wisconsin-Madison, Madison, WI 53706

CORRESPONDING AUTHOR:
Aaron A. Hoskins, ahoskins@wisc.edu

ORCID:
Sierra L. Love, 0000-0003-3254-9009
Aaron A. Hoskins, 0000-0002-9777-519X
Hai Dang Nguyen, 0000-0002-4200-8778

KEYWORDS: pre-mRNA splicing, high-throughput screen, inhibitors, modulators, yeast, SF3B1

ABSTRACT

Pre-mRNA splicing is a crucial process in eukaryotic gene expression, and splicing dysregulation has been linked to various diseases. However, very few small molecules have been discovered that can modulate spliced mRNA formation or inhibit the splicing machinery itself. This study presents a novel high-throughput screening (HTS) platform for identifying compounds that modulate splicing. Our platform comprises a two-tiered screening approach: a primary screen measuring growth inhibition in sensitized in *S. cerevisiae* (yeast) strains and a secondary screen that relies on production of a fluorescent protein as a readout for splicing inhibition. Using this approach, we identified 4 small molecules that cause accumulation of unspliced pre-mRNA *in vivo* in yeast. In addition, cancer cells expressing a myelodysplastic syndrome-associated splicing factor mutation ($SRSF2^{P95H}$) are more sensitive to one of these compounds than those expressing the wild-type version of the protein. Transcriptome analyses showed that this compound causes widespread changes in gene expression in sensitive $SRSF2^{P95H}$-expressing cells. Our results demonstrate the utility of using a yeast-based HTS to identify compounds capable of changing pre-mRNA splicing outcomes.

41 **INTRODUCTION**

42 Pre-mRNA splicing, the process of removing introns and joining exons to produce mature
43 mRNA molecules, is a critical regulatory step in eukaryotic gene expression. This essential process
44 is orchestrated by the spliceosome, a large ribonucleoprotein complex composed of five small
45 nuclear RNAs (snRNAs)—U1, U2, U4, U5, and U6—each associated with proteins to form small
46 nuclear ribonucleoproteins (snRNPs). Precise splicing is crucial for ensuring the production of
47 functional proteins that drive cellular function and organismal development. Dysregulation of pre-
48 mRNA splicing, whether through mutations in spliceosome components or alterations in RNA
49 substrates, has been linked to a broad spectrum of human diseases including cancers, neurological
50 disorders, and rare genetic syndromes[1].

51 Despite pre-mRNA splicing being studied for decades, there are few ways to chemically
52 modulate or inhibit splicing *in vivo* by targeting the splicing machinery itself[2]. This is especially
53 apparent when compared with the chemical tools available to inhibit protein translation at
54 numerous distinct stages[3]. Relatively few analogous chemical probes of splicing mechanism exist.
55 While it is possible to fuse tags to protein splicing factors to change their activity or abundance in
56 response to a small molecule (*e.g.,* degron tags)[4], only a handful of molecules have been discovered
57 that can change splicing by direct interaction with the endogenous machinery. The most widely
58 used splicing inhibitors are small molecules that target the U2 snRNP protein SF3B1. These
59 compounds (including pladienolide B, herboxidiene, and spliceostatin derivatives) are potent
60 inhibitors of splicing in humans by binding (sometimes covalently) to a protein pocket on SF3B1,
61 near its interaction site with the PHF5A protein[5]. The PHF5A protein can form a covalent adduct
62 with some of these inhibitors, leading to irreversible inhibition[6]. This pocket normally
63 accommodates the U2 snRNA/branch site intron RNA duplex, which cannot bind correctly if the

64 drug is present. Even though SF3B1 is overall highly conserved, yeast SF3B1 (Hsh155) is
65 naturally resistant to inhibition. Substitution of human for yeast Hsh155 protein domains or
66 mutation of the drug binding site in Hsh155 confers drug sensitivity[7, 8]. These mutated yeast strains
67 have subsequently been used for studies of splicing and intron structure due to their susceptibility
68 to specific and rapid splicing inhibition[9, 10]. A few other splicing inhibitors have been discovered
69 but are much less widely used and characterized and/or have controversial mechanisms of action[11].
70 In addition to their utility in laboratory settings, small molecule modulators of splicing can
71 show considerable clinical promise. This also has best been studied in terms of SF3B1-binding
72 compounds that have been used to selectively kill cancer cells with mutations in splicing factors,
73 such as those found in hematological malignancies[12, 13]. It is thought that dysregulated splicing,
74 accumulation of intronic RNA in the cytosol[13, 14], and other RNA metabolism abnormalities render
75 these cells uniquely sensitive to splicing modulation. This can create a therapeutic window that
76 spares normal cells[15, 16]. Alternatively, these drugs can be used to induce formation of novel protein
77 isoforms (proteoforms) via alternative splicing of transcripts, and the drug-dependent proteoforms
78 can in turn be used as cancer cell markers or for targeted neoantigen-based therapy[17].
79 In this study, we developed and validated a *Saccharomyces cerevisiae* (yeast)-based high-
80 throughput screening (HTS) platform for identifying small molecules that can change splicing
81 outcomes. We identified four compounds that function as splicing modulators *in vivo* in *S.*
82 *cerevisiae*. K562 cancer cells expressing the SRSF2^{P95H} splicing factor mutation are selectively
83 sensitive to one of these compounds, and drug treatment results in changes in gene expression and
84 splicing outcomes. Together, these findings highlight the utility of a yeast-based HTS for finding
85 new small molecule modulators of pre-mRNA splicing for potential biochemical and medical
86 applications.

87 **MATERIALS AND METHODS:**

88 **Chemicals and Drug Libraries**

89 Drug libraries include: Selleck Chem FDA-approved drugs, RIKEN-Pilot Natural Products
90 Depository (NPDepo), Life Chemicals 4 (LC4), and National Cancer Institute's (NCI)
91 Developmental Therapeutics Program (DTP) and Experimental Program (NExT) Diversity
92 libraries. Phleomycin and herboxidiene were diluted in water and DMSO, respectively, then
93 aliquoted and stored at -20˚C. The chemical libraries were diluted in DMSO to a final
94 concentration of 10 mM and stored at -80˚C.

95 **Preparation of Plasmids and Yeast Strains**

96 Wild-type (WT) and humanized Hsh155 plasmids and corresponding yeast strains have been
97 previously described[7, 8]. The plasmid BRR2 pRS313 (Addgene 111411; Guthrie lab) was modified
98 to remove three EcoRI sites, one SacI site, and add an AflII site using Quikchange Lightning Multi
99 (Agilent). These modifications facilitated further plasmid alterations without causing amino acid
100 changes in Brr2. The resulting plasmid (pAAH1347) is referred to as wild type (WT). Plasmid
101 pAAH1459 was created by PCR amplification of pAAH1347 to produce a 10.8 kb linear fragment
102 using Herculase II (Agilent). This fragment was combined with a synthetic gBlock encoding
103 humanized Brr2 regions using NEBuilder HiFi. The exchanged regions spanned from amino acids
104 L1202 to L1300 and L1540 to V1741. To construct Brr2 strains for plasmid shuffling and
105 screening, three ABC transporters (PDR5, YOR1, SNQ2) were sequentially deleted from strain
106 BY4741 using a CRISPR-based approach[18], resulting in the removal of the entire ORF of each
107 transporter without cloning scars or genomic incorporation of resistance markers. The resulting
108 strain (yAAH3007) was transformed with either pAAH1347 or pAAH1459, and transformants
109 were selected on synthetic dropout (SD) media lacking uracil (SD-URA). The genomic copy of

110 BRR2 was replaced with the hphMX6 gene cassette encoding hygromycin resistance through
111 homologous recombination[19].

112 Reporter plasmids containing genes for fluorescent proteins with introns were generously
113 provided by the Manny Ares lab (UCSC) and based on the modular yeast toolkit for gene
114 assembly[20]. Briefly, the plasmid constructs contain a kanamycin resistance cassette, URA3 marker,
115 and URA3 homology regions flanking a reporter gene driven by the PGK1 promoter. This
116 produces an RNA transcript with the PGK1 5' UTR, an open reading frame (ORF) encoding an N-
117 terminally FLAG and 6xHis-tagged yellow fluorescent protein (Venus), and the ADH1 3' UTR.
118 The ORFs were interrupted with introns based on the first intron of MATa1. Two different reporters
119 were used: (1) the splicing-in-frame (SPLIF) reporter in which the splicing of the pre-mRNA
120 removes the intron to leave a mRNA that properly codes for the Venus protein and (2) the splicing-
121 out-of-frame (SPLOOF) reporter in which intron removal causes a change in the reading from the
122 protein and lack of Venus production.

123 Plasmids were linearized with NotI to allow integration at the URA3 locus and selection
124 on -URA dropout plates. Linearized DNA was purified by agarose gel electrophoresis [1% (w/v)
125 low-melt agarose] followed by a Promega SV Gel and PCR Cleanup kit to remove the DNA from
126 the agarose. The linear DNA fragment was then transformed into yeast strains using standard
127 techniques[21] and selection carried out by plating on -URA DO plates. Correct integration was
128 confirmed by PCR and sequencing of the gene isolated from the modified yeast strains.

129 **Primary Screening of Drug Libraries**

130 Screening was conducted at the University of Wisconsin Carbone Cancer Center Small
131 Molecule Screening Facility (SMSF). Controls (DMSO, herboxidiene, and phleomycin) and

132 library compounds were dispensed into 384-well clear plates (Greiner Bio-One) using an Echo550
133 liquid handler.

134 Yeast strains were cultured overnight in DO-Trp (for Hsh155 strains) or DO-His (for Brr2
135 strains) liquid media with shaking at 220 rpm at 30°C. Before screening, the cells were diluted to
136 an optical density at 600nm (OD_{600}) of 0.1 and then grown to log phase (OD_{600} ~1.0) under the
137 same conditions. The culture was then diluted to an OD_{600} of 0.0075 in low nitrogen media made
138 by using yeast nitrogen base lacking both amino acids and ammonium sulfate and by addition of
139 1 g/L monosodium glutamate along with the appropriate mix of amino acids and nucleotides to
140 select for growth[22].

141 The diluted yeast were then added to 384-well plates (50µL per well; Greiner Bio-One)
142 using a BioTek Microflo Select liquid handler. Cells were incubated in a shaking incubator (220
143 rpm at 30°C) for 24 h. After incubation, cells were centrifuged at 1000g for 1 minute to remove
144 air bubbles and shaken at 2000 rpm for 4 min to ensure uniform readings in each well. Plates were
145 then read using a PHERAstar (BMG LABTECH) plate reader.

146 The Bland-Altman approach[23] was used to assess the reproducibility of yeast growth
147 between replicates. In summary, the differences between replicates and the mean growth values
148 were calculated for each well. These values were then plotted, and the upper and lower 95%
149 confidence limits were determined to represent the maximum variability between replicates.
150 Analysis of normalized growth data indicated that the differences between yeast growth replicates
151 ranged from -0.2 to 0.1, demonstrating that growth was highly consistent across replicates.

152 The screen quality was evaluated by calculating the statistical Z' values, with Z' values
153 between 0.5 and 1.0 indicating a robust, high-quality assay [24]. All screenings resulted in plate Z'
154 values between 0.70 and 0.95. Collected data were uploaded to the Collaborative Drug Discovery

155 (CDD) database for quality control and normalization. Each drug library, except for the RIKEN
156 NPDepo and the NCI DTP, was screened once per strain, and compounds showing at least 30%
157 growth inhibition relative to the DMSO controls were then re-screened in duplicate (for a total of
158 three replicates for these compounds). The RIKEN library was screened in triplicate for all strains,
159 and the NCI DTP was screened in duplicate for all strains.

160 **Secondary Screening of Compounds that Inhibit Yeast Growth**

161 Yeast strains with integrated SPLIF or SPLOOF reporters were grown overnight in DO-
162 Trp or DO-His liquid media at 30˚C with shaking (220 rpm). Cells were then diluted to an OD_{600}
163 of 0.1 in their respective dropout media. A total of 99 µL of these cultures was combined with 1
164 µL of DMSO or a library compound dissolved in DMSO in a Corning Costar 96 or 384-well black
165 clear-bottom cell culture plate. All compounds were at a final concentration of 10 µM. The plates
166 were covered with Breathe-Easy® plate sealing membranes to minimize evaporation and then
167 incubated at 30˚C with shaking at 220 rpm for 24 hours in a Tecan Infinite M1000Pro plate reader.
168 Turbidity (OD_{600}) and fluorescence intensity (512 nm excitation, 535 nm emission) were measured
169 every 15 min. For data analysis, each condition was normalized to the DMSO control. Lead
170 candidates were identified as those that reproducibly increased normalized fluorescence intensity
171 (> 1.0) for the SPLOOF reporter and decreased intensity for the SPLIF reporter (< 1.0) for at least
172 ten consecutive cycles (~2.5 h). These screens were performed in duplicate for each compound.

173 **RT-PCR to Validate pre-mRNA Accumulation**

174 Yeast cell cultures were grown overnight in SD-Trp or SD-His liquid media and then
175 diluted to an OD_{600} of 0.5. Cells were then treated with each drug at the indicated concentration
176 (see below) while shaking at 220 rpm at 30˚C. After 10 h, samples were collected and pelleted.
177 RNA was extracted from yeast cells using the NucleoSpin® RNA extraction kit (Machery-Nagel).

178 Splicing of the endogenous MATa1 transcript was then assessed by reverse transcription and PCR
179 using RNA (150 ng) isolated from each sample and Promega Access RT-PCR System kit in 25 μL
180 reactions. RT-PCR results were analyzed using agarose (2% w/v) gel electrophoresis to separate
181 spliced and unspliced bands using 3-4 biological replicates. Gels were photographed and images
182 analyzed using the ImageQuant analysis toolbox (Cytiva). Band intensities were quantified to
183 calculate the percent spliced for each reaction (mRNA/(pre-mRNA + mRNA)). Statistical analyses
184 (student's *t*-test) were performed using Excel and GraphPad Prism.

185 ***In Vitro* Splicing Reactions**

186 Assays were conducted as previously described [25]. In brief, nuclear extracts (NE) were
187 prepared from HeLa cells grown in DMEM/F-12 1:1 and 5% (v/v) newborn calf serum. [^{32}P]-
188 radiolabeled G(5′)ppp(5′)G-capped AdML pre-mRNA substrate was generated by T7 run-off
189 transcription followed by denaturing polyacrylamide gel purification. Each reaction consisted of
190 potassium glutamate (60 mM), magnesium acetate (2 mM), ATP (2 mM), creatine phosphate (5
191 mM), tRNA (0.1 mg/ ml-1), HeLa nuclear extract (40% v/v), and pre-mRNA substrate (2 nM).
192 Reaction reagents were incubated with DMSO (1% v/v) and each drug at the corresponding
193 concentrations for 60 min at 30˚C. RNA was extracted using phenol-chloroform, precipitated using
194 ethanol, dissolved in deionized formamide, and then resolved on a denaturing acrylamide gel (7
195 M Urea, 15% (w/v) acrylamide).

196 **Cell culture**

197 The *SRSF2*^{P95H} mutation was introduced into its endogenous locus in K562 cells using CRISPR-
198 Cas9, generating *SRSF2*$^{P95H/+/+}$ cells. SRSF2^{WT} and SRSF2^{P95H} mutant K562 cells were
199 maintained in IMDM medium (Gibco, 12-440-079) supplemented with penicillin–streptomycin

200 (100 U/mL, Gibco, No. 15140122), GlutaMax (1%, Gibco, No. 35050061), and cultured in a
201 37°C/5% CO_2 incubator.

202 **Cell Viability Assays**

203 K562 SRSF2^{WT} and SRSF2^{P95H} isogenic cells were seeded in white flat-well 96-well plates
204 at a density of 200-300 cells per well[26]. Cells were treated with compounds (0-50 μM) or a DMSO
205 control for 7 days. Cell viability was subsequently determined using CellTiterGlo (Promega, Cat.
206 G7571) according to the manufacturer's instructions. The proportion of viable cells with drug
207 treatment was calculated relative to the DMSO control. A four-parameter non-linear fit of inhibitor
208 concentration vs. response was performed in GraphPad Prism v10.0 (GraphPad Software, San
209 Diego, CA; RRID:SCR_002798).

210 **RNA-seq Sample Preparation and Sequencing**

211 K562 SRSF2^{WT} and SRSF2^{P95H} isogenic cells (500,000 per condition) were seeded and
212 treated with 16.7 μM of C7 for 24 h. Total RNA was isolated using TRIzol® according to the
213 manufacturer's instructions (Zymo Research, Cat. R2072) with DNase I treatment. Quantification
214 was performed using a Qubit Flex Fluorometer (Thermo Fisher Scientific). RNA quality control,
215 library preparation, and sequencing were performed by GENEWIZ (Azenta Life Sciences).
216 Library prep involved poly-(A) selection, cDNA synthesis, and adapter ligation. Sequencing was
217 completed on an Illumina® NovaSeq™ platform with a target depth of ~50-70 million paired-end
218 150 bp reads per sample. Data are available via the NCBI Sequence Read Archive (BioProject ID
219 PRJNA1271094).

220 **RNA-seq Data Analysis**

221 Sequence reads were trimmed to remove adapter sequences and nucleotides with poor
222 quality using Trimmomatic v0.36. The trimmed reads were mapped to the *Homo sapiens* GRCh38

223 reference genome available on ENSEMBL using the STAR aligner v2.5.2b. Unique gene hit counts
224 were obtained using featureCounts from the Subread package v1.5.2. GENEWIZ (Azenta Life
225 Sciences) performed trimming, alignment, and gene count quantification. Differential gene
226 expression analysis was conducted with DESeq2 v1.46.0 [27]. Genes were considered differentially
227 expressed (DEG) if they met the thresholds of $\log_2$ fold change > 1 or < -1 and an adjusted *p*-value
228 < 0.05. Alternative splicing (AS) analysis was performed using rMATS[28]. Differentially spliced
229 events were identified using a percent spliced-in (ΔPSI) change > 0.1 (10%) and a false discovery
230 rate (FDR) < 0.05. Functional enrichment analysis of significant DEGs and alternatively spliced
231 genes was conducted using ShinyGo with enriched Gene Ontology (GO) terms identified against
232 the human genome background[29].

233 **RESULTS AND DISCUSSION**

234 **Primary Screen Development and Optimization**

235 To identify molecules that act as splicing modulators, we first aimed to select compounds
236 that result in growth inhibition of yeast since pre-mRNA splicing is essential for viability. We
237 developed a primary screen to assay growth in 384-well plates in which the growth endpoint was
238 measured after 24 h (**Fig. 1B**). In order to bias for selection of splicing modulators, we utilized
239 yeast strains containing variant, non-native splicing factors. We chose to screen strains containing
240 either WT or "humanized" genes for Hsh155/SF3B1 or Brr2 proteins (**Fig. 1C**).

241 We focused on these proteins since they have already proven susceptible to drug targeting
242 in human cells[15, 30, 31]. We reasoned that use of these strains might lead to identification of
243 compounds that modulate splicing due to sensitization from lack of the endogenous splicing
244 machinery. Alternatively, this could lead to potential identification of compounds that target SF3B1
245 or Brr2 proteins directly. Further, we have already shown that yeast-human chimeras of

246 Hsh155/SF3B1 confer sensitivity to splicing modulators and growth inhibition, allowing us to use
247 these strains and compounds as positive controls during development of the screening
248 methodology. In the case of Hsh155/SF3B1, the protein was humanized by exchange of heat
249 repeats 5-16 of the yeast protein for the corresponding human domains (**Fig. 1C**) as previously
250 described[7, 8]. Brr2's domain organization consists of two helicase cassette modules. In this case,
251 we humanized the domain interface between these modules (**Fig. 1C**). This region is less well-
252 conserved between yeast and humans and is the binding site for allosteric inhibitors of Brr2
253 activity[30]. Finally, we utilized yeast strains lacking multi-drug efflux pumps and grew yeast in low-
254 nitrogen media in order to maximize sensitivity to compounds[8, 22, 32].

255 We next optimized yeast growth conditions in the high-density 384-well plates. In
256 preliminary studies, we grew humanized (Hs-Hsh155) and WT Hsh155 (WT-Hsh155) strains at
257 various starting concentrations (based on OD_{600}) with 0.1% v/v dimethyl sulfoxide (DMSO). We
258 found that wells inoculated to a starting OD_{600} of 0.0075 resulted in excellent well-to-well
259 consistency and reproducible growth after 24 h (**Fig. 1E**).

260 We then identified concentrations of phleomycin and herboxidiene that would achieve
261 maximum growth inhibition under these conditions for use as positive controls. Using the 384-
262 well plate format, we assayed concentration gradients of phleomycin (**Fig. 1F**; an anti-microbial
263 that should prevent growth of all the yeast strains used in these studies) and herboxidiene (**Fig.
264 1G**; a splicing inhibitor that should prevent growth of the Hs-Hsh155 strain but not others). We
265 found that robust growth inhibition could be obtained using concentrations of 16 μg/mL or 2 μM
266 of phleomycin or herboxidiene, respectively.

267 **Pilot Screening of FDA-Approved Drugs**

268 To evaluate this approach, we first screened the Selleck Chem FDA-approved drug library,
269 which contains 1078 chemically diverse compounds. This screen was conducted in duplicate using
270 the WT and Hs-Hsh155 yeast strains with the primary objective being to assess the sensitivity and
271 specificity of yeast growth as a readout for identifying compounds of interest. As a basis for
272 selecting potential growth inhibitors, we decided to choose those that reproducibly inhibited yeast
273 growth in at least one strain by ≥ 30% relative to the corresponding DMSO controls.

274 Using this approach, we identified 18 compounds that inhibited yeast growth in at least one
275 of the strains (**Fig. 1H, I**). Many of these are known antifungal drugs (*e.g.,* caspofungin,
276 clotrimazole); so, their identification was expected. In addition to antifungals, we also identified
277 members of other drug classes, including an antidepressant, immunosuppressants, a cognition-
278 enhancing medication, and an antihistamine (**Supp. Table S1**). Importantly, the assay's positive
279 controls, phleomycin and herboxidiene were successfully identified, while the negative control,
280 DMSO, was not. Herboxidiene was also identified only in the humanized, Hs-Hsh155 strain, not
281 the WT-Hsh155 strain. These findings highlight the platform's capability to not only identify
282 compounds that inhibit yeast growth but also distinguish between compounds that selectively
283 inhibit growth of one yeast strain over another via splicing modulation.

284 **Primary Screen Results**

285 Based on results from the Selleck FDA-approved drug library, we expanded our screen to
286 involve approximately 35,000 compounds sourced from four structurally diverse libraries: the
287 RIKEN-Pilot Natural Products Depository (NPDepo), Life Chemicals 4 (LC4), and National
288 Cancer Institute's (NCI) Developmental Therapeutics Program (DTP) and Experimental Program
289 (NExT) Diversity libraries. We also included the WT-Brr2 and Hs-Brr2 strains in the screen in
290 addition to WT-Hsh155 and Hs-Hsh155. In these screens, we calculated a Z' factor for each plate

291 to assess screen reliability [24]. Z' values were calculated using responses from wells containing
292 DMSO controls (no growth inhibition) vs. phleomycin (strong growth inhibition). All plate Z'
293 factor values exceed the cutoff of 0.5, indicating a high-quality screen (**Fig. 2A**).

294 Due to the sizes of the LC4 and NCI NExT libraries, we conducted an initial screen using
295 all four strains and then selected compounds that showed $\geq$ 30% growth inhibition. We then
296 screened these selected compounds a further two times, and those that consistently inhibited
297 growth by at least 30% were designated as "hits" from the primary screens of these libraries. For
298 the NCI DTP and RIKEN libraries, we screened the entire libraries three times in all four yeast
299 strains. In total, 379 compounds were identified based on our metrics (**Fig. 2B**). We then separated
300 the compounds based on which strain(s) growth inhibition was observed (**Fig. 2C**). While some
301 compounds (88) appeared to have general growth inhibitory properties for yeast and inhibited
302 growth of all strains, most of the compounds were selective for inhibiting growth in just one strain
303 or a subset. This suggests that the chosen yeast strains were indeed sensitized to different
304 compounds.

305 We further assessed the drug-likeness of these hits by investigating their structural and
306 physicochemical properties. Using *in silico* cheminformatics analysis with SwissADME[33], we
307 clustered the lead candidates according to Lipinski's rule of five parameters[34] : molecular weight
308 <500 g/mol, log$P$ < 5 (where P is the partition coefficient in octanol vs. water), proton donors < 5,
309 and proton acceptors < 10 (**Fig. 2D**). Approximately 70% of the hits demonstrated potential drug-
310 likeness, possessing the chemical and physical properties conducive to oral bioavailability. We
311 were unable to evaluate hits obtained from the Riken drug library due to lack of provided structural
312 information. Finally, we analyzed the hits in terms of their potential presence as false positives by
313 identifying any that are among the Pan Assay Interference Compounds (PAINS) class, which often

314 appear as frequent hits in HTS assays[35]. The majority of our hits (91%) pass PAINS criteria,
315 meaning they are not members of this class.

316 **Secondary Screen Optimization and Results**

317 We next developed a secondary screen to discriminate between compounds in which
318 growth inhibition is correlated with accumulation of unspliced pre-mRNAs and those which cause
319 growth inhibition but do not generally inhibit splicing. We incorporated a fluorescent protein
320 reporter gene (Venus) at the endogenous *URA3* locus in the WT-Hsh155, Hs-Hsh155, WT-Brr2,
321 and Hs-Brr2 strains. We employed two different reporter gene constructs (**Fig. 3A**, **B**): SPLIF
322 (splicing-in-frame) and SPLOOF (splicing-out-of-frame). The SPLIF reporter serves as a control,
323 generating a Venus protein upon translation of the spliced mRNA. In contrast, when splicing is
324 inhibited, Venus expression diminishes due to the inclusion of the intron and disruption of the
325 reading frame (**Fig. 3A**). Conversely, the SPLOOF reporter only allows for the Venus protein
326 production if the pre-mRNA is not spliced and the intron is retained (**Fig. 3B**). Thus, splicing
327 modulators can be identified by observing decreases in fluorescence due to loss of Venus protein
328 production in SPLIF-containing strains and increases in fluorescence due to production of Venus
329 protein in SPLOOF-containing strains.

330 To validate this secondary screen, we measured changes in both cell culture fluorescence
331 (normalized to the DMSO control) and optical density for 24 h for Hs-Hsh155 strains containing
332 SPLIF or SPLOOF reporters in the presence of DMSO, phleomycin, or herboxidiene (**Fig. 3C**, **D**).
333 As expected, we observed significant growth inhibition, as measured by the OD_{600}, for these strains
334 in the presence of phleomycin (16 μg/mL) or herboxidiene (2 μM) but not in the presence of
335 DMSO (shown in **Fig. 3C** Hs-Hsh155-SPLOOF). In the presence of herboxidiene, we observed a
336 transient increase in fluorescence lasting from ~1-7h during drug treatment for the strain carrying

337 the SPLOOF reporter and a corresponding decrease in fluorescence from the strain with the SPLIF
338 reporter. In contrast, we only observed decreases in fluorescence when cells were exposed to
339 phleomycin. These results show that addition of a known splicing modulator can cause changes in
340 culture fluorescence using the SPLIF/SPLOOF reporter system.

341 To verify that cellular pre-mRNA was indeed accumulating upon treatment with
342 herboxidiene, we used RT-PCR to determine relative abundances of unspliced and spliced
343 junctions for the first intron of endogenous MATa1 transcript (**Fig. 3E**). These results confirmed
344 that herboxidiene was causing unspliced transcript accumulation in the Hsh155- and Brr2-
345 modified yeast strains. Interestingly, we could also observe some accumulation of the unspliced
346 RNA in strains not expected to be sensitive to herboxidiene (WT-Hsh155 and the Brr2-modified
347 strains), albeit to a lower level than the sensitized strain (Hs-Hsh155). This suggests that
348 herboxidiene can at least partially inhibit yeast pre-mRNA splicing under these conditions, even
349 when little-to-no growth inhibition is observed. This is consistent with results recently reported by
350 Hunter and colleagues[9].

351 We then used this fluorescence-based screen to assay all 379 compounds identified in the
352 primary screen in eight different yeast strains (Hsh155- and Brr2-modified strains, each with either
353 the SPLIF or SPLOOF reporter) in duplicate. In each case, yeast were exposed to the compounds
354 for a total of 24 h. We used a threshold for splicing modulation as the presence of a normalized
355 (relative to DMSO) fluorescence intensity signal > 1.0 for stains with the SPLOOF reporter along
356 with a signal of < 1.0 for the corresponding condition with the SPLIF reporter. In addition, we
357 selected for compounds that caused changes in fluorescence that lasted at least for ten consecutive
358 cycles of measurement, or ~2.5h. From the starting set of 379 compounds, we identified 11 that
359 met all secondary screening criteria (**Supp. Table S2**).

360 When analyzing these compounds, we noted that the RIKEN library was the only one that
361 did not yield any secondary hits (**Fig. 4A**). Hits were evenly distributed among the other libraries
362 with no particular library more likely to contain a hit than any other based only on the distribution
363 of the primary screen hits. In terms of total library compounds, the greatest hit rates were obtained
364 from the NCI NeXT and DTP libraries (*cf.* **Fig. 2B**, **Fig. 4A**). Among the 11 hits, one structural
365 scaffold was represented by multiple hits: adenosine analogs. Both 3'-deoxyadenosine
366 (cordycepin) and 9-β-D-erythrofuranosyladenine (EFA), resulted in changes in splicing reporter
367 fluorescence in all of the tested strains (**Fig. 4B**, **C**; **Supp. Table S2**). Additional scaffolds included
368 benzothiazoles and benzoxazoles, which showed some strain specificity in the Hs-Brr2 (oxazoles)
369 and WT-Hsh155 (thiazole) backgrounds. Other hits were structurally unique, and their strain
370 specificities are detailed in Supplementary Table S2.

371 **Additional Validation and Characterization of Secondary Screen Hits**

372 To further confirm the splicing modulatory potential of the 11 hits, we assessed removal of
373 the first intron of the endogenous MATa1 transcript by RT-PCR for each compound in the WT-
374 Hsh155, Hs-Hsh155, WT-Brr2, and Hs-Brr2 strains. We compared the effects of each compound
375 to herboxidiene and DMSO controls. Four of the 11 compounds that passed secondary screening
376 demonstrated significant splicing inhibition of the endogenous MATa1 transcript (**Fig. 4C**, **D**).
377 Cordycepin, EFA, and compound C7 caused the most substantial accumulation of unspliced RNA
378 in the Hs-Hsh155 strain, while compound C8 reduced splicing efficiency in WT-Brr2 and Hs-Brr2
379 strains. It is possible that the remaining 7 compounds also inhibit splicing of other RNAs besides
380 that in the MATa1 transcript tested here; however, we did not explore this further. Nonetheless, we
381 conclude that our screen was successfully able to identify yeast splicing modulators that function
382 *in vivo* and that the efficacies of these modulators are strain-dependent.

383 **Splicing Factor Mutant Cancer Cells are Sensitive to Compound C7**

384 Finally, we decided to test if any of the identified compounds also exhibited splicing
385 modulatory activity in human cells. Previous studies have demonstrated that cancer cells harboring
386 mutant splicing factors are more susceptible to splicing modulation than their WT counterparts[36].
387 Inspired by this, we tested four compounds (those shown in **Fig. 4C**) for antiproliferative activity
388 against isogenic K562 cancer cells expressing either wildtype SRSF2 or the hematologic
389 malignancy-associated *SRSF2*^{P95H} mutation[26]. Cells were treated with increasing concentrations of
390 each drug, and relative cell viability was assessed after seven days. We did not find any significant
391 differences in antiproliferative activity for cordycepin, EFA, or compound C8 between the
392 SRSF2^{WT} and SRSF2^{P95H} cells (data not shown). However, we observed the SRSF2^{P95H} cells
393 exhibited reduced proliferation relative to SRSF2^{WT} cells in response to compound C7 (**Fig. 5A**,
394 **B**). We note that compound C7 has been reported as a potential luciferase inhibitor[37], which could
395 interfere with the proliferation assay. However, we did not detect any inhibition of luciferase
396 activity in control experiments using the Cell-TiterGlo kit (data not shown).

397 **Compound C7 Does Not Generally Inhibit pre-mRNA Splicing *in vitro* but Changes Gene**
398 **Expression *in vivo***

399 To further explore the mechanism by which SRSF2-mutant cells are sensitive to compound
400 C7, we analyzed pre-mRNA splicing *in vitro* and *in vivo*. We were unable to observe any significant
401 reduction in splicing of the well-characterized AdML pre-mRNA substrate in human HeLa cell
402 nuclear extract (a standard extract and substrate for *in vitro* assays of the human splicing
403 machinery) at concentrations up to 200 μM of compound C7 (**Supp. Fig. S1**). This suggests that
404 either compound C7 does not target the core splicing machinery directly or that any impact on

405 splicing may be cell type or transcript-specific and not able to be reconstituted *in vitro* using this
406 extract and/or substrate.

407 To assess transcriptome changes caused by compound C7 in K562 cells, we carried out
408 RNA sequencing on poly-A selected RNA isolated from SRSF2 WT or P95H mutant cells after
409 exposure to DMSO or C7 (16.7 μM for 24h). We first analyzed the results in terms of differentially
410 expressed genes (DEGs), which we defined as those with a $\log_2$-fold change of < -1
411 (downregulated) or > 1 (upregulated) and an adjusted p-value < 0.05.

412 As expected, the most prominent changes in DEG occurred in comparison of the SRSF2
413 WT and P95H mutant cells even in the absence of drug treatment (**Supp. Fig. S2**). This is
414 consistent with previous findings that the $SRSF2^{P95H}$ mutation by itself alters gene expression and
415 splicing[38].

416 When comparing each strain's response to C7, we found that C7 caused relatively few
417 uniquely downregulated DEGs in the $SRSF2^{P95H}$ mutant cells relative to $SRSF2^{WT}$ (15 DEGs, **Fig.**
418 **5C**). However, it resulted in many more upregulated genes in the $SRSF2^{WT/P95H}$ cells including
419 those involved in regulation of apoptosis and cell death (248 DEGs; **Fig. 5C**, **D**). It is possible that
420 dysregulation of this process leads to the decrease in proliferation observed in $SRSF2^{WT/P95H}$ cells
421 relative to WT upon treatment with C7.

422 **Changes in pre-mRNA Splicing due to Treatment with Compound C7**

423 We then looked at the changes in splicing due to compound C7 using rMATS to perform
424 differential splicing analysis[28]. Again, consistent with prior studies, we observed many changes in
425 splicing due to the $SRSF2^{P95H}$ mutation itself, even in the absence of compound treatment (**Fig.**
426 **6A**)[38]. The most common event types were skipped exons; however, we also observed changes in
427 retained introns, mutually exclusive exons, and splice site usage. To visualize changes occurring

428 specifically in the SRSF2 mutant cells upon compound treatment, we created Venn diagrams to
429 quantify the numbers of unique events (**Fig. 6B-F**). This analysis revealed that while many of the
430 same types of changes in alternative splicing due to the P95H mutation are observed in both DMSO
431 and C7-treated cells, treatment with C7 resulted in unique splicing outcomes. For example, while
432 $SRSF2^{P95H}$ mutant cells showed nearly 2000 skipped exon events relative to WT under both DMSO
433 and C7 conditions, the vast majority of these events were non-identical. Approximately 75%
434 (~1500) of the skipped exon events attributed to the P95H mutation observed in DMSO were not
435 observed upon C7 treatment and *vice versa* (**Fig. 6B**). The same was true for other types of
436 alternative splicing events (**Fig. 6C-F**). GO-term analysis of the genes with alternative splicing
437 events unique to the SRSF2 P95H mutant cells upon C7 treatment relative to WT showed that the
438 splicing changes impacted a wide range of processes especially those involving gene expression
439 including transcriptional regulation, DNA and RNA metabolism, and translation (**Supp. Table S3**).
440 As with upregulation of genes involved in apoptosis, dysregulation of mRNA isoform generation
441 could lead to the observed proliferative defects in the $SRSF2^{P95H}$ mutant cells. In summary, we
442 conclude that compound C7 modulates splicing in $SRSF2^{WT}$ and $SRSF2^{P95H}$ mutant cells
443 differently with transcriptome-wide impacts that may result in impaired cellular proliferation.

444 **CONCLUSION**

445 In this work, we created a yeast cell-based high-throughput screening platform that
446 identified four *in vivo* splicing modulators. These compounds inhibit growth of *S. cerevisiae* and
447 can cause accumulation of unspliced MATa1 transcripts in yeast. Further analysis of these
448 compounds demonstrated that one, compound C7, reduces proliferation of K562 cells harboring
449 the cancer-associated $SRSF2^{P95H}$ mutation and that these splicing factor-mutant cells are more
450 sensitive to this compound than their wildtype counterparts. The increased sensitivity could be due

451 to changes in regulation of genes involved in processes such as apoptosis and/or reprogramming
452 of alternative splicing.

453 A significant advantage of our screening platform is its simplicity, cost-effectiveness, and
454 scalability. Unlike mammalian cell-based assays, our yeast system can be easily set-up on a lab
455 bench without needing a biosafety cabinet. Yeasts grow much more rapidly than mammalian cells
456 and in much less expensive growth media. This allows for facile, low-cost, and rapid identification
457 of splicing modulators. A limitation of our studies is that we have not identified the precise targets
458 of these compounds in yeast or human cells. It is possible that these compounds may exert their
459 effects via indirect mechanisms. For example, by changing transcription, chromatin structure, or
460 RNA export. It is interesting to note that two of the identified compounds, cordycepin and EFA,
461 are adenosine analogs. We speculate that these could inhibit splicing by associating with nucleotide
462 binding pockets within the splicing machinery (such as the branch site adenosine pocket on
463 Hsh155/SF3B1)[39] by interfering with ATP binding to the highly conserved splicesomal ATPases
464 [40] or by indirectly impacting splicing through changes in coupled RNA processing events such as
465 transcription or polyadenylation. Future work could focus on target deconvolution for these
466 molecules as well as expanding studies of C7 for potential therapeutic applications.

467 **Acknowledgments**

468 SLL, HV, and AAH were funded by a EvansMDS Discovery research grant from the Edward P.
469 Evans Foundation. SLL was supported by the Genetics Training Program (NIH 5T32GM007133)
470 and the SciMed Graduate Research Scholars Fellowship. YCC was supported by the Targets of
471 Cancer Training Program (NIH T32CA009138). MSJ was supported by the National Institutes of
472 Health (R01GM72649). HDN is supported by grants from the Masonic Cancer Center, Edward P.
473 Evans Foundation, American Society of Hematology, the NIH's National Heart, Lung, and Blood

Institute (R01HL163011), and the 2022 AACR Career Development Award to Further Diversity, Equity, and Inclusion in Cancer Research, which is supported by Merck, grant number 22–20–68-NGUY. We thank the UW-Madison small molecule screening facility for instrument access. We also thank Dr. Manny Ares for splicing reporter plasmids. Finally, we thank Laura Vanderploeg for figure editing.

References

(1) Dvinge, H.; Kim, E.; Abdel-Wahab, O.; Bradley, R. K. RNA splicing factors as oncoproteins and tumour suppressors. *Nat Rev Cancer* **2016**, *16* (7), 413–430. DOI: 10.1038/nrc.2016.51 From NLM Medline. Love, S. L.; Emerson, J. D.; Koide, K.; Hoskins, A. A. Pre-mRNA splicing-associated diseases and therapies. *RNA Biol* **2023**, *20* (1), 525–538. DOI: 10.1080/15476286.2023.2239601 From NLM Medline.

(2) Effenberger, K. A.; Urabe, V. K.; Jurica, M. S. Modulating splicing with small molecular inhibitors of the spliceosome. *Wiley Interdiscip Rev RNA* **2017**, *8* (2), 19. DOI: 10.1002/wrna.1381 From NLM Medline.

(3) Dmitriev, S. E.; Vladimirov, D. O.; Lashkevich, K. A. A Quick Guide to Small-Molecule Inhibitors of Eukaryotic Protein Synthesis. *Biochemistry (Mosc)* **2020**, *85* (11), 1389–1421. DOI: 10.1134/S0006297920110097 From NLM Medline.

(4) Ji, T.; Yang, Y.; Yu, J.; Yin, H.; Chu, X.; Yang, P.; Xu, L.; Wang, X.; Hu, S.; Li, Y.; et al. Targeting RBM39 through indisulam induced mis-splicing of mRNA to exert anti-cancer effects in T-cell acute lymphoblastic leukemia. *J Exp Clin Cancer Res* **2024**, *43* (1), 205. DOI: 10.1186/s13046-024-03130-8 From NLM Medline. Singh, S.; Quarni, W.; Goralski, M.; Wan, S.; Jin, H.; Van de Velde, L. A.; Fang, J.; Wu, Q.; Abu-Zaid, A.; Wang, T.; et al. Targeting the spliceosome through RBM39 degradation results in exceptional responses in high-risk neuroblastoma models. *Sci Adv* **2021**, *7* (47), eabj5405. DOI: 10.1126/sciadv.abj5405 From NLM PubMed-not-MEDLINE. Xu, Y.; Nijhuis, A.; Keun, H. C. RNA-binding motif protein 39 (RBM39): An emerging cancer target. *Br J Pharmacol* **2022**, *179* (12), 2795–2812. DOI: 10.1111/bph.15331 From NLM Medline.

(5) Cretu, C.; Agrawal, A. A.; Cook, A.; Will, C. L.; Fekkes, P.; Smith, P. G.; Luhrmann, R.; Larsen, N.; Buonamici, S.; Pena, V. Structural Basis of Splicing Modulation by Antitumor Macrolide Compounds. *Mol Cell* **2018**, *70* (2), 265–273 e268. DOI: 10.1016/j.molcel.2018.03.011 From NLM Medline.

(6) Cretu, C.; Gee, P.; Liu, X.; Agrawal, A.; Nguyen, T. V.; Ghosh, A. K.; Cook, A.; Jurica, M.; Larsen, N. A.; Pena, V. Structural basis of intron selection by U2 snRNP in the presence of covalent inhibitors. *Nat Commun* **2021**, *12* (1), 4491. DOI: 10.1038/s41467-021-24741-1 From NLM Medline.

(7) Carrocci, T. J.; Paulson, J. C.; Hoskins, A. A. Functional analysis of Hsh155/SF3b1 interactions with the U2 snRNA/branch site duplex. *RNA* **2018**, *24* (8), 1028–1040. DOI: 10.1261/rna.065664.118 From NLM Medline.

(8) Hansen, S. R.; Nikolai, B. J.; Spreacker, P. J.; Carrocci, T. J.; Hoskins, A. A. Chemical Inhibition of Pre-mRNA Splicing in Living Saccharomyces cerevisiae. *Cell Chem Biol* **2019**, *26* (3), 443–448 e443. DOI: 10.1016/j.chembiol.2018.11.008 From NLM Medline.

(9) Hunter, O.; Talkish, J.; Quick-Cleveland, J.; Igel, H.; Tan, A.; Kuersten, S.; Katzman, S.; Donohue, J. P.; M, S. J.; Ares, M., Jr. Broad variation in response of individual introns to splicing inhibitors in a humanized yeast strain. *RNA* **2024**, *30* (2), 149–170, Article. DOI: 10.1261/rna.079866.123 From NLM Medline.

(10) Rangan, R.; Huang, R.; Hunter, O.; Pham, P.; Ares, M.; Das, R. RNA structure landscape of *S. cerevisiae* introns. *bioRxiv* **2024**, 2022.2007.2022.501175. DOI: 10.1101/2022.07.22.501175.

(11) Lazear, M. R.; Remsberg, J. R.; Jaeger, M. G.; Rothamel, K.; Her, H. L.; DeMeester, K. E.; Njomen, E.; Hogg, S. J.; Rahman, J.; Whitby, L. R.; et al. Proteomic discovery of chemical probes that perturb protein complexes in human cells. *Mol Cell* **2023**, *83* (10), 1725–1742 e1712. DOI: 10.1016/j.molcel.2023.03.026 From NLM Medline. Tellier, M.; Ansa, G.; Murphy, S. Isoginkgetin and Madrasin are poor splicing inhibitors. *PLoS One* **2024**, *19* (10), e0310519. DOI: 10.1371/journal.pone.0310519 From NLM Medline. Sidarovich, A.; Will, C. L.; Anokhina, M. M.; Ceballos, J.; Sievers, S.; Agafonov, D. E.; Samatov, T.; Bao, P.; Kastner, B.; Urlaub, H.; et al. Identification of a small molecule inhibitor that stalls splicing at an early step of spliceosome activation. *Elife* **2017**, *6*. DOI: 10.7554/eLife.23533 From NLM Medline.

(12) Fuentes-Fayos, A. C.; Pérez-Gómez, J. M.; G-García, M. E.; Jiménez-Vacas, J. M.; Blanco-Acevedo, C.; Sánchez-Sánchez, R.; Solivera, J.; Breunig, J. J.; Gahete, M. D.; Castaño, J. P.; et al. SF3B1 inhibition disrupts malignancy and prolongs survival in glioblastoma patients through BCL2L1 splicing and mTOR/ß-catenin pathways imbalances. *Journal of Experimental & Clinical Cancer Research 2022 41:1* **2022**, *41* (1). DOI: 10.1186/s13046-022-02241-4. Lopez-Oreja, I.; Gohr, A.; Playa-Albinyana, H.; Giro, A.; Arenas, F.; Higashi, M.; Tripathi, R.; Lopez-Guerra, M.; Irimia, M.; Aymerich, M.; et al. SF3B1 mutation-mediated sensitization to H3B-8800 splicing inhibitor in chronic lymphocytic leukemia. *Life Sci Alliance* **2023**, *6* (11), 25. DOI: 10.26508/lsa.202301955 From NLM Medline. Maji, D.; Grossfield, A.; Kielkopf, C. L. Structures of SF3b1 reveal a dynamic Achilles heel of spliceosome assembly: Implications for cancer-associated abnormalities and drug discovery. *Biochim Biophys Acta Gene Regul Mech* **2019**, *1862* (11-12), 194440. DOI: 10.1016/j.bbagrm.2019.194440 From NLM Medline.

(13) Seiler, M.; Yoshimi, A.; Darman, R.; Chan, B.; Keaney, G.; Thomas, M.; Agrawal, A. A.; Caleb, B.; Csibi, A.; Sean, E.; et al. H3B-8800, an orally available small-molecule splicing modulator, induces lethality in spliceosome-mutant cancers. *Nat Med* **2018**, *24* (4), 497–504. DOI: 10.1038/nm.4493 From NLM Medline.

(14) Bowling, E. A.; Wang, J. H.; Gong, F.; Wu, W.; Neill, N. J.; Kim, I. S.; Tyagi, S.; Orellana, M.; Kurley, S. J.; Dominguez-Vidana, R.; et al. Spliceosome-targeted therapies trigger an antiviral immune response in triple-negative breast cancer. *Cell* **2021**, *184* (2), 384–403 e321. DOI: 10.1016/j.cell.2020.12.031 From NLM Medline. Agrawal, A. A.; Yu, L.; Smith, P. G.; Buonamici, S. Targeting splicing abnormalities in cancer. *Curr Opin Genet Dev* **2018**, *48*, 67–74. DOI: 10.1016/j.gde.2017.10.010 From NLM Medline.

(15) Dart, A. Targeting aberrant splicing. *Nat Rev Cancer* **2023**, *23* (10), 653, Editorial Material; Early Access. DOI: 10.1038/s41568-023-00620-3 From NLM PubMed-not-MEDLINE.

(16) Wheeler, E. C.; Martin, B. J. E.; Doyle, W. C.; Neaher, S.; Conway, C. A.; Pitton, C. N.; Gorelov, R. A.; Donahue, M.; Jann, J. C.; Abdel-Wahab, O.; et al. Splicing modulators impair DNA damage response and induce killing of cohesin-mutant MDS and AML. *Sci Transl Med* **2024**, *16* (728), eade2774. DOI: 10.1126/scitranslmed.ade2774 From NLM Medline. Yamauchi, H.; Nishimura, K.; Yoshimi, A. Aberrant RNA splicing and therapeutic opportunities in cancers. *Cancer Sci* **2022**, *113* (2), 373–381. DOI: 10.1111/cas.15213 From NLM Medline.

(17) Lu, S. X.; De Neef, E.; Thomas, J. D.; Sabio, E.; Rousseau, B.; Gigoux, M.; Knorr, D. A.; Greenbaum, B.; Elhanati, Y.; Hogg, S. J.; et al. Pharmacologic modulation of RNA splicing enhances anti-tumor immunity. *Cell* **2021**, *184* (15), 4032–4047 e4031. DOI: 10.1016/j.cell.2021.05.038 From NLM Medline. Kim, W. J.; Crosse, E. I.; De Neef, E.; Etxeberria, I.; Sabio, E. Y.; Wang, E.; Bewersdorf, J. P.; Lin, K. T.; Lu, S. X.; Belleville, A.; et al. Mis-splicing-derived neoantigens and cognate TCRs in splicing factor mutant leukemias. *Cell* **2025**. DOI: 10.1016/j.cell.2025.03.047 From NLM Publisher.

(18) Owens, D. D. G.; Caulder, A.; Frontera, V.; Harman, J. R.; Allan, A. J.; Bucakci, A.; Greder, L.; Codner, G. F.; Hublitz, P.; McHugh, P. J.; et al. Microhomologies are prevalent at Cas9-induced larger deletions. *Nucleic Acids Res* **2019**, *47* (14), 7402–7417. DOI: 10.1093/nar/gkz459 From NLM Medline.

(19) Goldstein, A. L.; McCusker, J. H. Three new dominant drug resistance cassettes for gene disruption in Saccharomyces cerevisiae. *Yeast* **1999**, *15* (14), 1541–1553. DOI: 10.1002/(SICI)1097-0061(199910)15:14<1541::AID-YEA476>3.0.CO;2-K From NLM Medline.

(20) Lee, M. E.; DeLoache, W. C.; Cervantes, B.; Dueber, J. E. A Highly Characterized Yeast Toolkit for Modular, Multipart Assembly. *ACS Synth Biol* **2015**, *4* (9), 975–986. DOI: 10.1021/sb500366v From NLM Medline.

(21) Amberg, D. C.; Burke, D. J. Classical Genetics with Saccharomyces cerevisiae. *Cold Spring Harb Protoc* **2016**, *2016* (5). DOI: 10.1101/pdb.top077628 From NLM Medline.

(22) Cheng, T. H.; Chang, C. R.; Joy, P.; Yablok, S.; Gartenberg, M. R. Controlling gene expression in yeast by inducible site-specific recombination. *Nucleic Acids Res* **2000**, *28* (24), E108. DOI: 10.1093/nar/28.24.e108 From NLM Medline.

(23) Bland, J. M.; Altman, D. G. Statistical methods for assessing agreement between two methods of clinical measurement. *Lancet* **1986**, *1* (8476), 307–310. From NLM Medline.

(24) Zhang, J. H.; Chung, T. D.; Oldenburg, K. R. A Simple Statistical Parameter for Use in Evaluation and Validation of High Throughput Screening Assays. *J Biomol Screen* **1999**, *4* (2), 67–73. DOI: 10.1177/108705719900400206 From NLM Publisher.

589 (25) Effenberger, K. A.; Perriman, R. J.; Bray, W. M.; Lokey, R. S.; Ares, M., Jr.; Jurica, M. S. A
590 high-throughput splicing assay identifies new classes of inhibitors of human and yeast
591 spliceosomes. *J Biomol Screen* **2013**, *18* (9), 1110–1120. DOI: 10.1177/1087057113493117 From
592 NLM Medline.

593 (26) Liu, Z. S.; Sinha, S.; Bannister, M.; Song, A.; Arriaga-Gomez, E.; McKeeken, A. J.; Bonner,
594 E. A.; Hanson, B. K.; Sarchi, M.; Takashima, K.; et al. R-Loop Accumulation in Spliceosome
595 Mutant Leukemias Confers Sensitivity to PARP1 Inhibition by Triggering Transcription-
596 Replication Conflicts. *Cancer Res* **2024**, *84* (4), 577–597. DOI: 10.1158/0008-5472.CAN-23-3239
597 From NLM Medline.

598 (27) Love, M. I.; Huber, W.; Anders, S. Moderated estimation of fold change and dispersion for
599 RNA-seq data with DESeq2. *Genome Biology* **2014**, *15* (12). DOI: 10.1186/s13059-014-0550-8.

600 (28) Shen, S.; Park, J. W.; Lu, Z. X.; Lin, L.; Henry, M. D.; Wu, Y. N.; Zhou, Q.; Xing, Y. rMATS:
601 robust and flexible detection of differential alternative splicing from replicate RNA-Seq data. *Proc*
602 *Natl Acad Sci U S A* **2014**, *111* (51), E5593–5601. DOI: 10.1073/pnas.1419161111 From NLM
603 Medline.

604 (29) Ge, S. X.; Jung, D.; Yao, R. ShinyGO: a graphical gene-set enrichment tool for animals and
605 plants. *Bioinformatics* **2020**, *36* (8), 2628–2629. DOI: 10.1093/bioinformatics/btz931 From NLM
606 Medline.

607 (30) Iwatani-Yoshihara, M.; Ito, M.; Klein, M. G.; Yamamoto, T.; Yonemori, K.; Tanaka, T.; Miwa,
608 M.; Morishita, D.; Endo, S.; Tjhen, R.; et al. Discovery of Allosteric Inhibitors Targeting the
609 Spliceosomal RNA Helicase Brr2. *J Med Chem* **2017**, *60* (13), 5759–5771. DOI:
610 10.1021/acs.jmedchem.7b00461 From NLM Medline.

611 (31) Ito, M.; Iwatani, M.; Yamamoto, T.; Tanaka, T.; Kawamoto, T.; Morishita, D.; Nakanishi, A.;
612 Maezaki, H. Discovery of spiro[indole-3,2'-pyrrolidin]-2(1H)-one based inhibitors targeting Brr2,
613 a core component of the U5 snRNP. *Bioorg Med Chem* **2017**, *25* (17), 4753–4767, Article. DOI:
614 10.1016/j.bmc.2017.07.017 From NLM Medline. Effenberger, K. A.; Urabe, V. K.; Prichard, B.
615 E.; Ghosh, A. K.; Jurica, M. S. Interchangeable SF3B1 inhibitors interfere with pre-mRNA splicing
616 at multiple stages. *RNA* **2016**, *22* (3), 350–359. DOI: 10.1261/rna.053108.115 From NLM
617 Medline.

618 (32) McMurray, M. A.; Thorner, J. Septin stability and recycling during dynamic structural
619 transitions in cell division and development. *Curr Biol* **2008**, *18* (16), 1203–1208. DOI:
620 10.1016/j.cub.2008.07.020 From NLM Medline.

621 (33) Daina, A.; Michielin, O.; Zoete, V. SwissADME: a free web tool to evaluate
622 pharmacokinetics, drug-likeness and medicinal chemistry friendliness of small molecules. *Sci Rep*
623 **2017**, *7*, 42717. DOI: 10.1038/srep42717 From NLM Medline.

624 (34) Lipinski, C. A.; Lombardo, F.; Dominy, B. W.; Feeney, P. J. Experimental and computational
625 approaches to estimate solubility and permeability in drug discovery and development settings.

Adv Drug Deliv Rev **2001**, *46* (1-3), 3–26. DOI: 10.1016/s0169-409x(00)00129-0 From NLM Medline. Lipinski, C. A. Drug-like properties and the causes of poor solubility and poor permeability. *J Pharmacol Toxicol Methods* **2000**, *44* (1), 235–249. DOI: 10.1016/s1056-8719(00)00107-6 From NLM Medline.

(35) Baell, J. B.; Holloway, G. A. New substructure filters for removal of pan assay interference compounds (PAINS) from screening libraries and for their exclusion in bioassays. *J Med Chem* **2010**, *53* (7), 2719–2740. DOI: 10.1021/jm901137j From NLM Medline.

(36) Pellagatti, A.; Boultwood, J. Splicing factor mutations in the myelodysplastic syndromes: Role of key aberrantly spliced genes in disease pathophysiology and treatment. *Adv Biol Regul* **2023**, *87*, 100920. DOI: 10.1016/j.jbior.2022.100920 From NLM Medline. Lee, S. C.; Dvinge, H.; Kim, E.; Cho, H.; Micol, J. B.; Chung, Y. R.; Durham, B. H.; Yoshimi, A.; Kim, Y. J.; Thomas, M.; et al. Modulation of splicing catalysis for therapeutic targeting of leukemia with mutations in genes encoding spliceosomal proteins. *Nat Med* **2016**, *22* (6), 672–678. DOI: 10.1038/nm.4097 From NLM Medline.

(37) PubChem Compound Summary for CID 833827, 4-Amino-2-[5-(propan-2-yl)-1,3-benzoxazol-2-yl]phenol. https://pubchem.ncbi.nlm.nih.gov/compound/833827 (accessed.

(38) Jia, W.; Guo, X.; Wei, Y.; Liu, J.; Can, C.; Wang, R.; Yang, X.; Ji, C.; Ma, D. Clinical and prognostic profile of SRSF2 and related spliceosome mutations in patients with acute myeloid leukemia. *Mol Biol Rep* **2023**, *50* (8), 6601–6610. DOI: 10.1007/s11033-023-08597-w From NLM Medline. Kim, E.; Ilagan, J. O.; Liang, Y.; Daubner, G. M.; Lee, S. C.; Ramakrishnan, A.; Li, Y.; Chung, Y. R.; Micol, J. B.; Murphy, M. E.; et al. SRSF2 Mutations Contribute to Myelodysplasia by Mutant-Specific Effects on Exon Recognition. *Cancer Cell* **2015**, *27* (5), 617–630. DOI: 10.1016/j.ccell.2015.04.006 From NLM Medline. Rahman, M. A.; Lin, K. T.; Bradley, R. K.; Abdel-Wahab, O.; Krainer, A. R. Recurrent SRSF2 mutations in MDS affect both splicing and NMD. *Genes Dev* **2020**, *34* (5-6), 413–427. DOI: 10.1101/gad.332270.119 From NLM Medline. Zhang, J.; Lieu, Y. K.; Ali, A. M.; Penson, A.; Reggio, K. S.; Rabadan, R.; Raza, A.; Mukherjee, S.; Manley, J. L. Disease-associated mutation in SRSF2 misregulates splicing by altering RNA-binding affinities. *Proc Natl Acad Sci U S A* **2015**, *112* (34), E4726–4734. DOI: 10.1073/pnas.1514105112 From NLM Medline.

(39) van der Feltz, C.; Hoskins, A. A. Structural and functional modularity of the U2 snRNP in pre-mRNA splicing. *Crit Rev Biochem Mol Biol* **2019**, *54* (5), 443–465. DOI: 10.1080/10409238.2019.1691497 From NLM Medline.

(40) Staley, J. P.; Guthrie, C. Mechanical devices of the spliceosome: motors, clocks, springs, and things. *Cell* **1998**, *92* (3), 315–326. DOI: 10.1016/s0092-8674(00)80925-3 From NLM Medline.

\

Figures and Legends

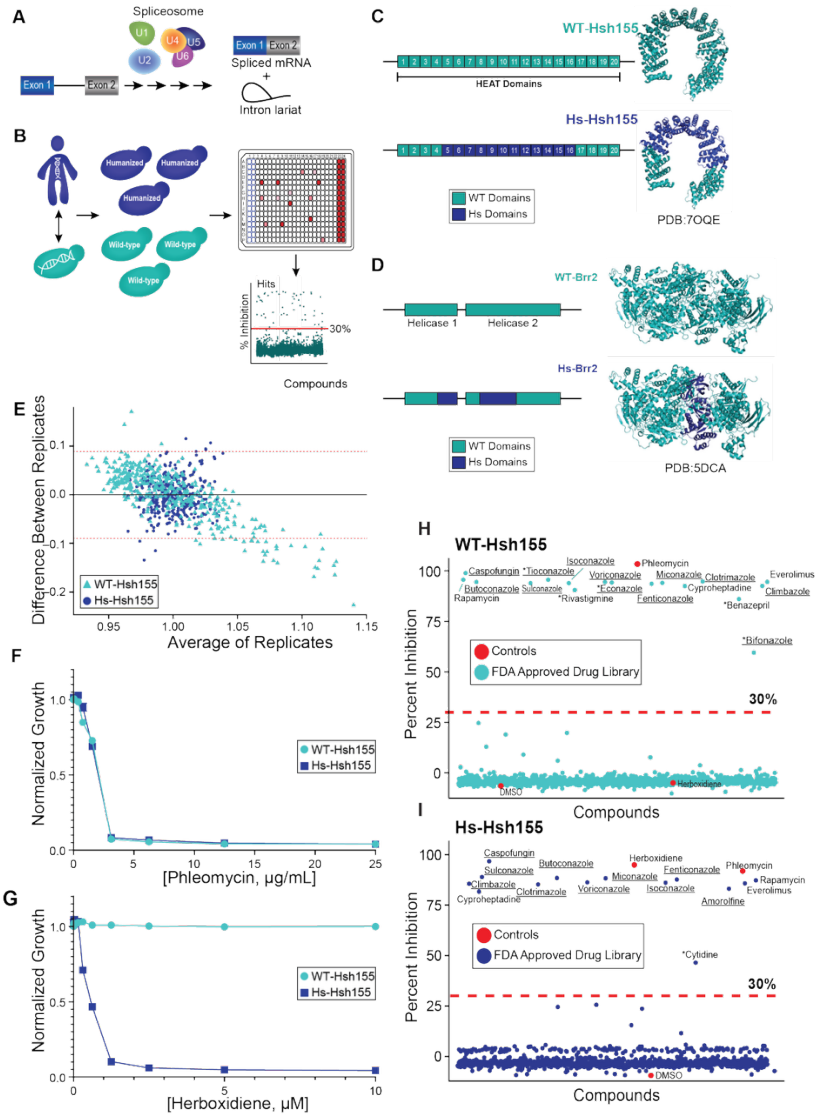

Figure 1. Primary Screen Development and Optimization (A) Overview of pre-mRNA splicing: introns are removed and exons joined to generate mature mRNA. This process is catalyzed by the spliceosome, composed of five small nuclear ribonucleoproteins (U snRNPs). **(B)** Schematic of primary screening strategy. Compounds were screened in 384-well plates using wild-type and humanized yeast strains. Hits were identified as those that reduced yeast growth by ≥ 30% relative to DMSO controls. **(C, D)** Diagrams of chimeric Hsh155 and Brr2 proteins used in engineered yeast strains. **(E)** Bland-Altman plot assessing reproducibility between biological replicates. Red dotted lines indicate 95% confidence limits. Both the x- and y-axes are expressed in terms of absorbance (OD_{600}) units. **(F, G)** Dose-response curves of controls (phleomycin and herboxidiene) in WT and Hs-Hsh155 yeast. Relative growth was measured at 24 h post-treatment and normalized to DMSO controls. **(H, I)** Pilot screen of Selleck Chem FDA-approved drug library. Percent growth inhibition of Hsh155 strains relative to DMSO controls are shown; red dotted lines indicate 30% inhibition thresholds. Antifungals are underlined; strain-specific hits are marked with asterisks.

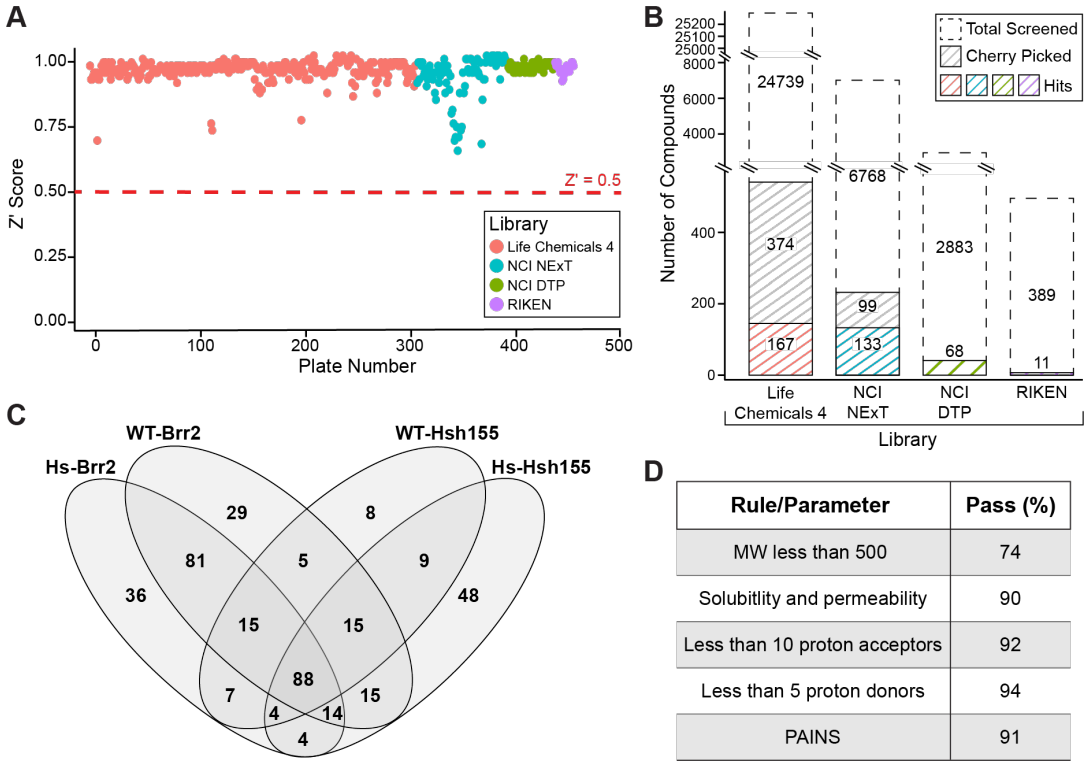

D

Rule/Parameter	Pass (%)
MW less than 500	74
Solubitlity and permeability	90
Less than 10 proton acceptors	92
Less than 5 proton donors	94
PAINS	91

Figure 2. **Primary Screen Results (A)** Scatterplot of Z' scores for each screening plate. Red dotted line marks the quality threshold (Z' = 0.5). Libraries are color-coded as indicated. **(B)** Stacked bar graph showing the number of compounds screened per library, categorized as total library compounds, those cherry-picked for subsequent replicates and rescreened but not identified as hits (grey diagonals), and primary hits (colored diagonals, which were derived from those that were cherry-picked for the Life Chemicals 4 and NCI NExT libraries). **(C)** Venn diagram illustrating overlap of primary hits across four yeast strains, highlighting shared and strain-specific compounds. **(D)** Table summarizing the percentage of primary hits that meet Lipinski's Rule of Five and PAINS (Pan Assay Interference Compounds) filters.

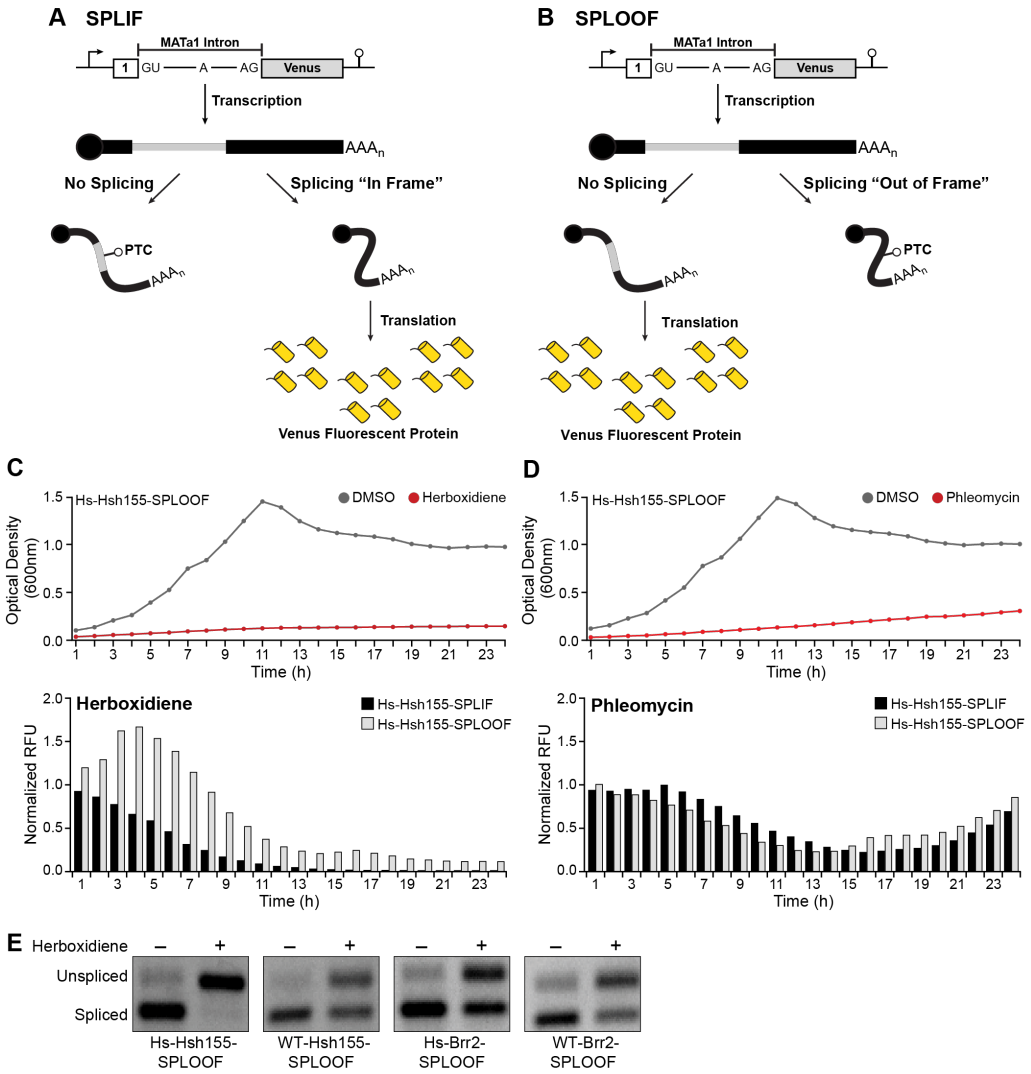

Figure 3. Secondary Screen Optimization (A, B) Schematic of splicing inhibition reporters used in secondary screening. Both constructs include the yeast MATa1 intron inserted into the ORF for the Venus fluorescent protein gene. In the SPLIF reporter, proper splicing produces high Venus fluorescence, which decreases with splicing inhibition. In the SPLOOF reporter, splicing disrupts the reading frame, suppressing Venus expression; splicing inhibition restores in-frame expression, increasing fluorescence. **(C, D)** (Top) Optical density measurement time courses (OD_{600}) of the Hs-Hsh155-SPLOOF strain upon treatment with either DMSO (grey) or herboxidiene or phleomycin (red). (Bottom) Fluorescence measurement time courses of Hs-Hsh155-SPLIF (black bars) or Hs-Hsh155-SPLOOF (grey bars) following treatment with 2 µM herboxidiene or 16 µg/mL phleomycin, normalized to DDMSO controls. **(E)** RT-PCR validation of splicing inhibition in SPLOOF strains treated with DMSO or 2 µM herboxidiene, confirming retention of the MATa1 first intron (unspliced band) upon addition of drug.

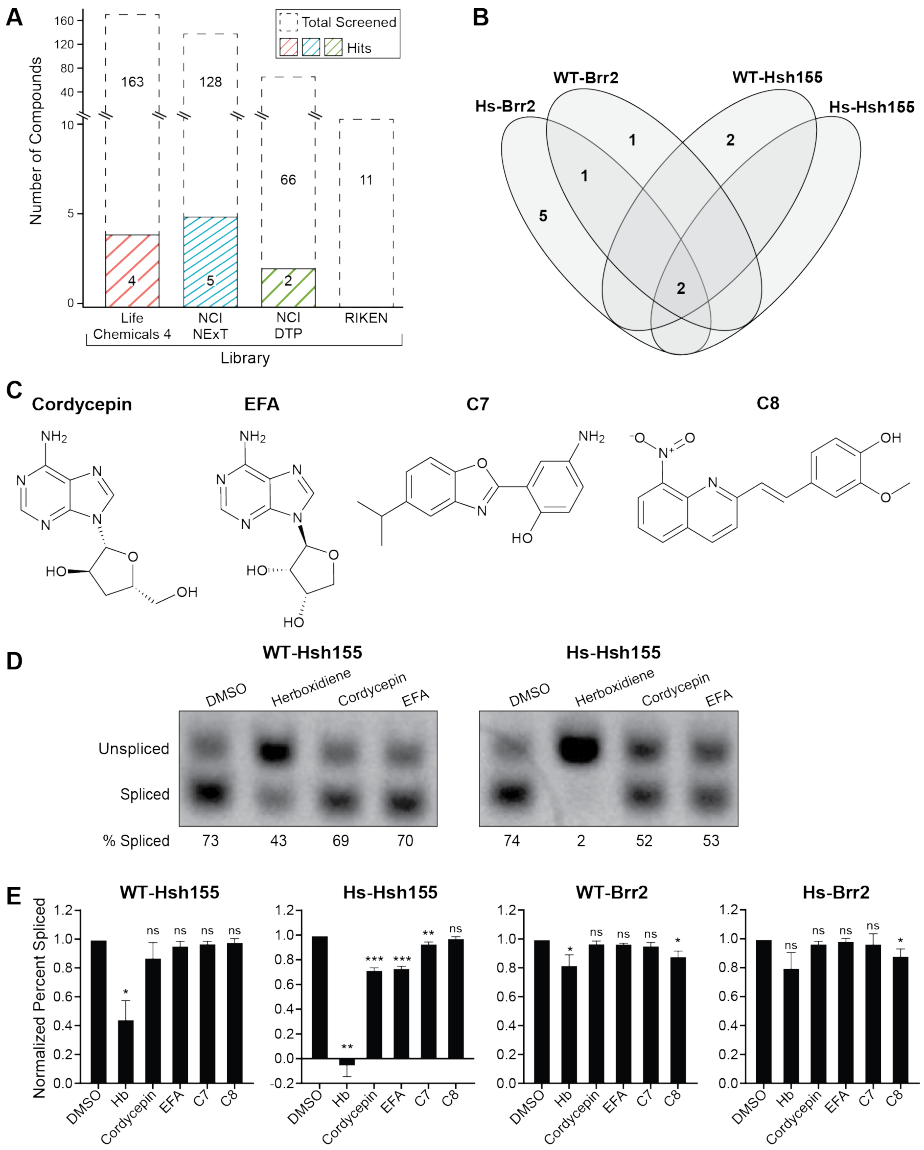

Figure 4. Secondary Screening Results (A) Stacked bar graph showing the number of compounds screened per library using the secondary screen and the corresponding number of hits. **(B)** Venn diagram showing overlap of secondary screen hits between strains. **(C)** Chemical structures of cordycepin, EFA, compound C7, and compound C8. **(D)** Representative RT-PCR results and quantification of the splicing of the endogenous MATa1 gene first intron in each strain treated with 10 µM of each compound. Values are normalized to DMSO. Error bars represent standard deviation (N= 3). Statistical significance of the effects of compound treatment vs. the DMSO controls was calculated using an unpaired two-tailed Welch's t-test (*$p < 0.05$, **$p < 0.005$, ***$p < 0.001$).

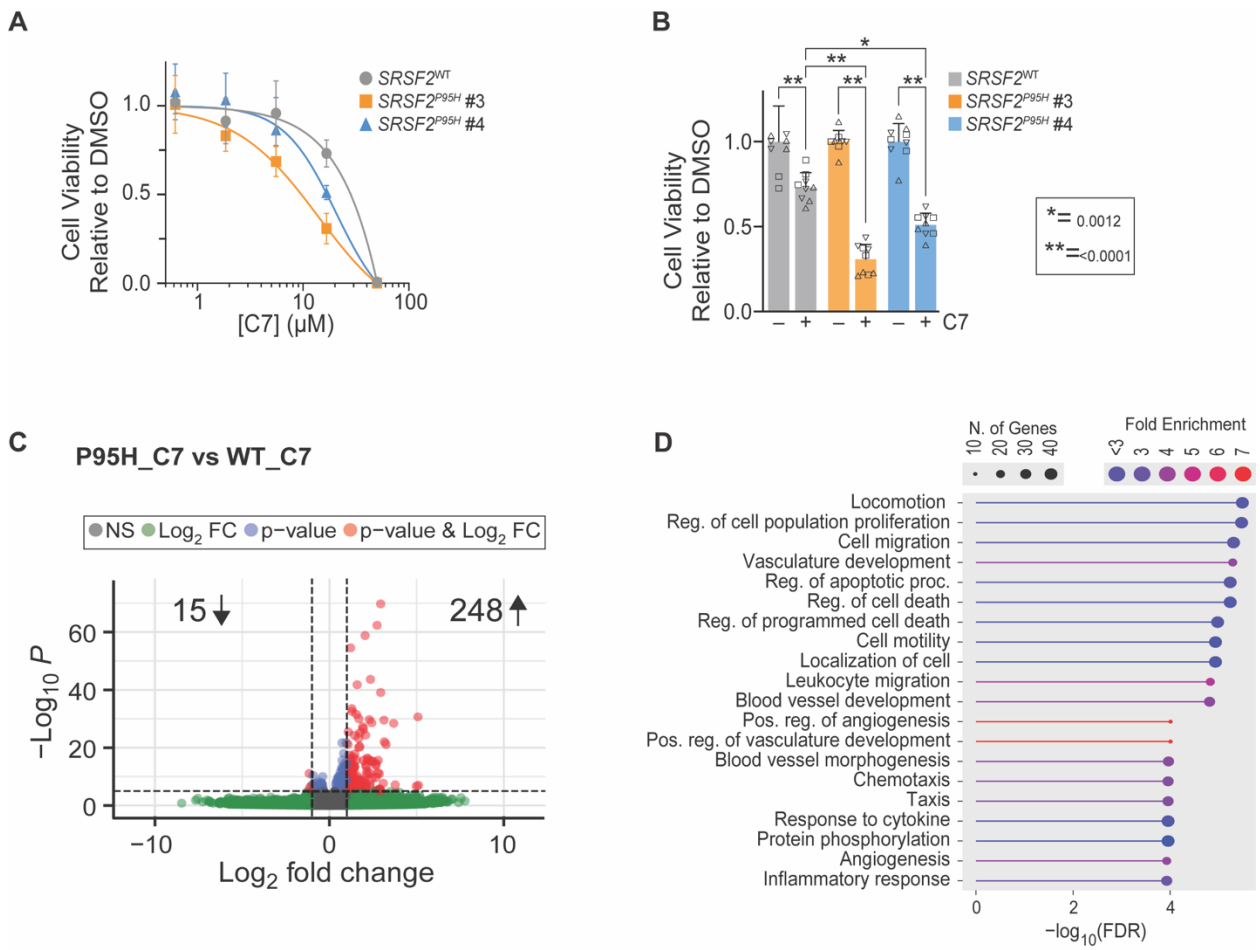

Figure 5. Splicing Mutant Cancer Cells are Sensitized to Compound C7 (A) Relative viability of K562 SRSF2$^{WT/WT}$ and SRSF2$^{WT/P95H}$ K562 cells in tissue culture treated with increasing concentrations of C7 for 7 days. Data points represent the mean of 3 biological replicates and error bars represent standard deviation. Two independently-obtained clones of the SRSF2$^{WT/P95H}$ cell line were tested (clones #3 and #4). (B) Relative survival of K562 SRSF2^{WT} and SRSF2^{P95H} treated with 16.7 μM of C7 for 7 days. Bars represent the mean of 9 technical replicates across 3 biological replicates and error bars represent standard deviation. Two-way ANOVA with Sidak's multiple comparison test. **(C)** Volcano plot displaying uniquely down (left side) and up-regulated DEGs (right side) in K562 SRSF2 $^{WT/P95H}$ cells vs. WT when treated with C7 relative to DMSO controls for each. DEGs were defined as those with $\log_2$ fold change < -1 or >1 and a -$\log_{10}$ *p*-value >0.05 (red dots). **(D)** Gene ontology (GO) enrichment analysis of the upregulated DEGs.

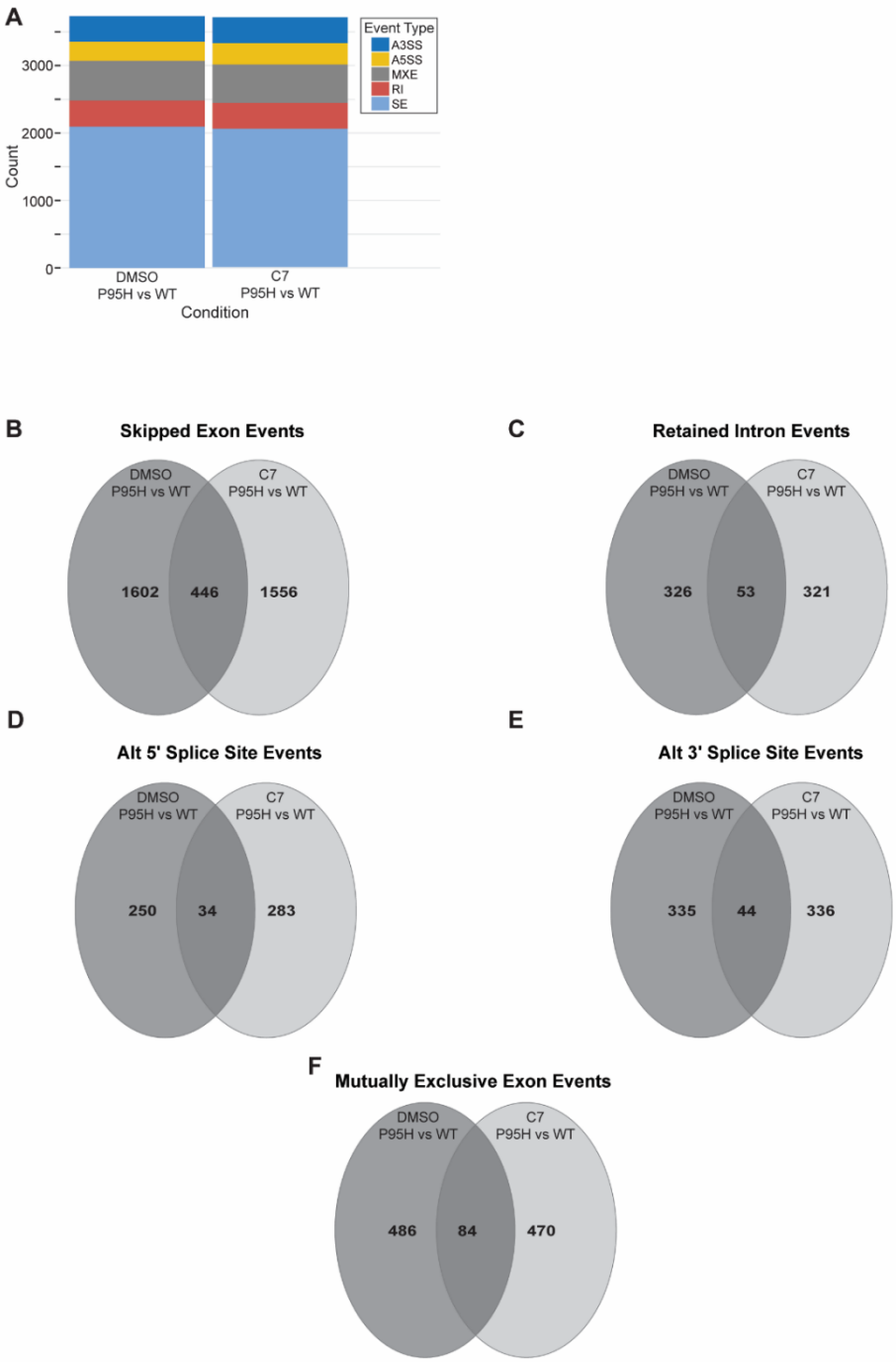

Figure 6. C7 Treatment Induces Changes in pre-mRNA Splicing (A) Stacked bar graph showing the distribution of novel alternative splicing events found in P95H mutant cells relative to WT after treatment with DMSO (left bar) and compound C7 (right bar). A3SS/A5SS: alternative 3'/5' splice sites; MXE: mutually exclusive exons; RI: retained introns; SE: skipped exons. **(B–F)** Venn diagrams showing unique splicing events in the P95H mutant cells in comparison to WT upon treatment with DMSO (dark gray) or compound C7 (light gray). Overlapping events were unique to the P95H cell line relative to WT and found upon treatment with either DMSO or C7.